Thermoresponsive Fluorescence Switches Based on Au@pNIPAM Nanoparticles

Dana Kamzabek, Brieuc Le Dé, Liliane Coche-Guérente, Fabien Miomandre, Galina V Dubacheva

Thermoresponsive Fluorescence Switches Based on Au@pNIPAM Nanoparticles

*Dana Kamzabek,[‡] Brieuc Le Dé,[‡] Liliane Coche-Guérente,[§] Fabien Miomandre[‡] and Galina V. Dubacheva [‡,§]**

[‡]PPSM, CNRS, Ecole Normale Supérieure Paris-Saclay, Université Paris-Saclay, 61 Avenue Président Wilson, 94235 Cachan, France. [§]Department of Molecular Chemistry, Univ. Grenoble Alpes, CNRS UMR 5250, 570 rue de la chimie, CS 40700, Grenoble 38000, France.

Corresponding author email: *galina.dubacheva@univ-grenoble-alpes.fr*

ABSTRACT

Despite numerous studies emphasizing the plasmonic impact on the fluorescence, the design of a dynamic system allowing on demand fluorescence switching in a single nanostructure remains challenging. The reversibility of fluorescence switching and the versatility of the approach, in particular its compatibility with a wide range of nanoparticles and fluorophores, are among the main experimental difficulties. In this work, we achieve reversible fluorescence switching by coupling metal nanoparticles with fluorophores through stimuli-responsive organic linkers. As a proof of concept, we link gold nanoparticles with fluorescein through thermo-responsive poly(N-isopropylacrylamide) at tunable grafting density and characterize their size and optical response by dynamic light scattering, absorption and fluorescence spectroscopies. We show that

fluorescence emission of these hybrid nanostructures can be switched on demand using the thermo-responsive properties of poly(N-isopropylacrylamide). The described system presents a general strategy for the design of nanointerfaces exhibiting reversible fluorescence switching *via* external control of metal nanoparticle/fluorophore distance.

INTRODUCTION

Thanks to their unique optoelectronic properties, high scaffold capacity, tunable morphology and well-established surface chemistry, metal nanoparticles (Me NPs) represent an attractive platform for applications in nanotechnology. [1–3] In particular, their functionalization with optically active molecules was shown to be promising for highly sensitive sensing such as SERS and "chemical nose" technologies. [2,3] Among different optical properties, luminescence stands out by its strong dependence on Me NP/fluorophore electronic interactions: adverse effects from quenching up to 1000-fold enhancement have been reported in static configurations. [4–6] Achieving luminescence variation in a single dynamic nanostructure whose configuration is switched on demand would boost nanotechnological applications. [7]

Conventional approaches to modulate luminescence in Me NP/fluorophore assemblies are mostly based on semiconducting NPs, conducting molecules or photochromic systems. [8–10] A new route has emerged recently through supramolecular chemistry, with only few examples of those fluorescence switches being reported. [11–16] These supramolecularly dynamic assemblies are compatible with a wide range of fluorophores, NPs and external stimuli. Their implementation in nanotechnologies is yet impaired by the irreversibility/low reproducibility of luminescence switching, necessity to add/remove soluble triggers, incompatibility with surface confinement

and, in some cases, biospecific nature of supramolecular interactions (e.g. protein-, DNA-based) limiting their potential applications to biological assays.

We propose to overcome these limitations by linking Me NPs with fluorophores through stimuli-responsive covalent organic linkers. We chose thermo-responsive poly(N-isopropylacrylamide) (pNIPAM) as a model polymeric linker. When dissolved in water, pNIPAM changes its conformation from swollen to collapsed upon heating to 32 °C. [17] This process is reversible, does not require injection of additional molecules and can occur in the presence of organic solvents as well as on surfaces. [17–19] Furthermore, previous studies have demonstrated that pNIPAM preserves its thermo-responsive behavior after grafting to Me NPs, with different potential applications being addressed using such hybrid systems, including optical lensing, SERS, colloidal actuation, biphasic catalysis, plasmon/meta-film tuning and biosensing. [13,20–26] These characteristics, together with the developed conjugation chemistries, make pNIPAM a straightforward candidate for the proof of concept.

In contrast to previously reported Me NP/pNIPAM fluorescence switches, in which fluorescent molecules were non-covalently trapped inside the pNIPAM shell through hydrophobic or electrostatic interactions,[13,15,16,27] we decided to link Me NPs with fluorophores covalently through bi-functional pNIPAM linker. Among the potential benefits of this strategy are: i) better control of the Me NP/fluorophore distance and fluorophore surface density due to the fixed position of the fluorophore at the extremity of the pNIPAM chain and possibility to tune pNIPAM grafting density, ii) higher robustness of the system due to the chemical attachment of all components and therefore low risk of fluorophore release and iii) possibility to adjust surface chemistry to specific biomedical applications by introducing additional functional groups (OEG, specific ligands, etc.). We used commercially available pNIPAM derivative bearing azide and

thiol functional groups from the opposite sides, which allowed stable anchoring to Me NPs and fluorophore covalent attachment in an orthogonal manner. Spherical Au NPs were chosen as metal nanostructures due to their well-known synthetic and surface chemistries and numerous applications in material and biomedical sciences. [1,2] 5-carboxyfluorescein (FAM) was chosen as a model fluorophore due to its large spectral overlap with the absorption of spherical Au NPs, high fluorescence quantum yield and solubility in aqueous media. [28] DLS, UV-visible and fluorescence spectroscopy were used to characterize the size, optical properties and stimuli-responsive behavior of the produced nano-assemblies. We showed that temperature-driven shrinking of the pNIPAM coating induces changes in the Au NP/FAM distance, thus allowing on-demand fluorescence switching at the nano-scale. The developed here approach allows reversible fluorescence modulation, does not require injection of soluble triggers and is compatible a wide range of fluorophores, nanoparticles and external stimuli, which makes it promising for a wide range of applications from multifunctional nanoprobes such as nanothermometers to renewable functional interfaces suitable for watermarking or mechanofluorochromic sensing.

EXPERIMENTAL SECTION

Synthesis of Au NPs. Au NPs were synthesized following the Turkevich method described in previous studies. [29,30] Briefly, 2 mL of the reducing aqueous solution containing 1% w/v trisodium citrate (77.5 μmol, Acros Organics) and 0.05% w/v citric acid (5.2 μmol, Alfa Aesar) was added into 50 mL of boiling water. After 15 min, 630 μL of 0.7% w/v aqueous solution of $H[AuCl_4]$ (12.8 μmol, Sigma-Aldrich) was injected under vigorous stirring. After 5 min of

boiling, the mixture was left to cool down for 1h. An Au NPs suspension was thus obtained and could be kept at 4 °C for a maximum of 3 weeks.

Calculation of Au NPs surface area. The total surface of Au NPs (s_{AuNP} in nm^2) in a given solution volume was calculated as $s_{\mathrm{AuNP}} = c_{\mathrm{AuNP}} \times N_A \times V_{\mathrm{soln}} \times 4\pi r^2$, where c_{AuNP} is the concentration of Au NPs in the solution (mol/L), N_A is the Avogadro's number (mol^{-1}), V_{soln} is the volume of solution (L) and r is the average radius of spherical Au NPs (nm). c_{AuNP} was calculated as $c_{\mathrm{AuNP}} = \frac{c_{\mathrm{Au}} \times Mw_{\mathrm{Au}}}{\rho_{\mathrm{Au}} V_{1\mathrm{AuNP}} N_A}$, where c_{Au} is the concentration of Au^0 in the synthesized Au NPs suspension (mol/L), Mw_{Au} is the atomic weight of Au (g/mol), ρ_{Au} is the density of Au (g/nm^3) and $V_{1\mathrm{AuNP}}$ is the volume of a single Au NP (nm^3). c_{AuNP} was determined spectroscopically based on the UV-Vis response of the synthesized Au NPs and using the reported extinction calibrations. [31,32]

Functionalization of pNIPAM with FAM. Chemical structure of the bifunctional pNIPAM derivative, bearing azide and protected thiol groups from the opposite sides, is shown in Fig. S1 (average M_n = 15000 g/mol, PDI ≤ 1.3, Sigma-Aldrich). Functionalization of the azide-terminated pNIPAM with 5-carboxyfluorescein alkyne (FAM-alkyne, 5-isomer, 97%, Lumiprobe, Fig. S1) and deprotection of the pNIPAM thiol group were done according to previously reported protocols. [33–37] FAM-alkyne was attached to pNIPAM through Cu(I)-catalyzed azide-alkyne cycloaddition reaction in aqueous medium. [33–35] Briefly, 850 µL of 8 mM FAM-alkyne solution (7.0 µmol) was added to 7.5 mL of 0.45 mM pNIPAM solution (3.5 µmol). Then, 24 mM solution of $CuSO_4$ (4.2 mL, 102.5 µmol, Acros Organics), 140 mM solution of sodium ascorbate (2.5 µL, 337 µmol, Sigma) and 41 mM solution of bathophenanthrolinedisulfonic acid disodium salt hydrate (5 mL, 202.5 µmol, Alfa Aesar) were added successively. All reagents were prepared in 0.1 M sodium phosphate buffer (pH 8). The

reaction occurred in the final volume of 20 mL overnight under Ar. The product was purified through successive dialysis (10 000 MW, Thermo Fisher) in 0.1 M sodium phosphate buffer (12 h), 0.01 M sodium phosphate buffer (2 x 24 h) and water (12 h). The purified product was recovered by freeze-drying and kept at 4 °C (47 mg, 86% yield). The efficiency of click functionalization was estimated by UV-visible spectroscopy (Fig. S2). pNIPAM-FAM concentration was determined according to the Beer-Lambert equation $c = A/\epsilon\, l$, where A is the measured at 464 nm absorbance of the pNIPAM-FAM solution (0.314), ϵ is the measured molar absorptivity of FAM in 0.1 M sodium phosphate buffer at pH 8 (31500 L mol^{-1} cm^{-1}) and l is the path length (1 cm). The isosbestic wavelength 464 nm was chosen to exclude the influence of the solution medium on the resulting absorbance of FAM. [38] Assuming that optical properties of FAM were not influenced by its grafting to pNIPAM (Fig. S3), the estimated yield of the click reaction was found to be 31 %. Thiol group of pNIPAM was deprotected by the previously reported aminolysis of the trithiocarbonate bond (Fig. 1S), which was optimized for 15 kDa pNIPAM. [36,37] Briefly, 50 mg of pNIPAM (3.3 μmol) was dissolved in 1.5 mL of anhydrous DMSO followed by the injection of 38 μL of tributylphosphine (150 μmol, Sigma-Aldrich). The solution was mixed at 40 °C for 2 h, after that 30 μL of isopropylamine (300 μmol, Acros Organics) was added, and the resulting solution was kept at 40 °C for additional 3 h. All reaction steps were performed under Ar. After cooling to room temperature (around 20 °C), the product was washed 3 times with an excess of diethyl ether and dried under Ar (48 mg, 97% yield). The chemical structure of the obtained thiolated pNIPAM-FAM is shown in Fig. 1A.

Assembly of Au NPs with pNIPAM. To study the effect of grafting density, different amounts of concentrated (typically 20-50 μM) pNIPAM-FAM aqueous solution were added into small volumes (5-10 mL) of citrate-stabilized Au NPs. The injected amounts corresponded to the

grafting densities of 0.1, 0.2, 0.5, 1.0 and 100 pNIPAM-FAM/nm^2. Au NPs suspension was used as synthesized, with typical Au^0 concentration of 0.26 mM and citrate in large excess (850 citrate/nm^2). pNIPAM-FAM was injected drop by drop under vigorous stirring and the resulting mixture was incubated overnight at room temperature (around 20 °C). For each ratio, the corresponding reference sample was prepared by injecting the same amount of pNIPAM-FAM into water. The solutions were protected from light by aluminum foil throughout the conjugation process. The nano-assemblies obtained at low grafting densities (0.1 - 1.0 pNIPAM-FAM/nm^2) were characterized within the next several days as prepared, i.e. without additional purification from pNIPAM-FAM. We note that according to the UV-visible characterization of pNIPAM-FAM (see the previous section), it represents a mixture of thiolated pNIPAM with (31%) and without (69%) FAM. Given the same solubility and close molecular weights of the two constructs, one may assume the efficiency of surface grafting to be similar for pNIPAM and pNIPAM-FAM.[39] We thus expect every third pNIPAM chain grafted to Au NPs to display FAM at the solution-facing interface.

Characterization techniques. DLS, UV-visible and fluorescence spectroscopic characterization was done at 20 °C in plastic cuvettes (path length = 1 cm, Kartell). Au NPs (c_{Au0} = 0.26 mM) were diluted 5- to 10-times. Samples were prepared in filtered (0.2 um pore size, Fisherbrand) ultrapure water. Additional DLS measurements, fluorescence spectra and fluorescence kinetics at tunable temperature were recorded in 10 mM sodium phosphate buffer (pH 8). When characterizing thermo-responsive properties, the samples were thermostated during 15 min upon heating to 40 °C and then again 15 min upon cooling to 20 °C. When comparing different dilutions, normalization was done by dividing the recorded values on the maximal intensity obtained for a given sample. DLS was done using the Zetasizer Nano-S instrument (Malvern)

equipped with a He-Ne laser and a detector located at 173°. UV-visible absorption spectroscopy was done using the double beam Varian Cary-4000 spectrophotometer (Agilent). Baseline recorded for water was subtracted from all spectra. Fluorescence excitation, emission and kinetics were recorded using Fluorolog-3 spectrofluorometer (Horiba Jobin-Yvon) equipped with 450 W xenon lamp. Fluorescence signal was corrected by removing the wavelength sensitivity of detectors. In addition, the reference detector was used to remove the temporary fluctuations caused by the lamp, giving the corrected signal-to-reference intensity in [CPS/MicroAmps]. Emission spectra were recorded in the range from 495 to 700 nm while exciting FAM at 480 nm wavelength. Excitation spectra were recorded in the range from 400 to 515 nm at the FAM emission wavelength fixed to 530 nm. Emission kinetics was recorded for the emission wavelength of 530 nm while exciting at 465 nm. AFM characterization was done in air using Thermo Microscope (Veeco). The topography images (Fig. S4) were recorded in tapping mode using silicon cantilevers (PPP-NCHR, Nanosensors) at typical resonance frequency of 300 kHz and force constant of 40 N/m. To prepare AFM samples, ITO-coated glass substrates (Solems, 80 nm thickness) were placed into the aqueous solution of citrate-stabilized Au NPs. After 15 h, the substrates were thoroughly rinsed with water and dried. No additional chemistry was applied to stabilize the immobilized Au NPs on the ITO surface.

Ultrapure (milli-Q) water was used for the preparation of all aqueous solutions. 0.1 M sodium phosphate buffer (pH 8) was prepared by mixing 18.64 mL of 1M Na_2HPO_4 solution with 1.36 mL of 1M NaH_2PO_4 solution and diluting the resulting mixture to 200 mL with water (salts were purchased from Sigma). The resulting pH = 8.0 ± 0.1 was verified with the pH meter, with no additional salts being added to adjust the obtained value. 0.01 M sodium phosphate buffer (pH 8) was prepared by diluting 0.1 M sodium phosphate buffer (pH 8) 10 times with water.

RESULTS AND DISCUSSION

Functionalization of pNIPAM with FAM was done through azide-alkyne click chemistry (Fig. 1A). The copper-catalyzed cycloaddition was performed according to the established protocols, where bathophenanthrolinedisulfonic acid was used as a Cu(I) stabilizing ligand suitable for azide-alkyne ligation in aqueous media. [19,40] The obtained pNIPAM-FAM was purified from free FAM by dialysis and characterized by UV-visible (Fig. S2) and fluorescence spectroscopy (Fig. 1B, black and green). The efficiency of pNIPAM functionalization with FAM was found to be 31% (see Methods and ESI for the details of pNIPAM functionalization and UV-visible characterization).

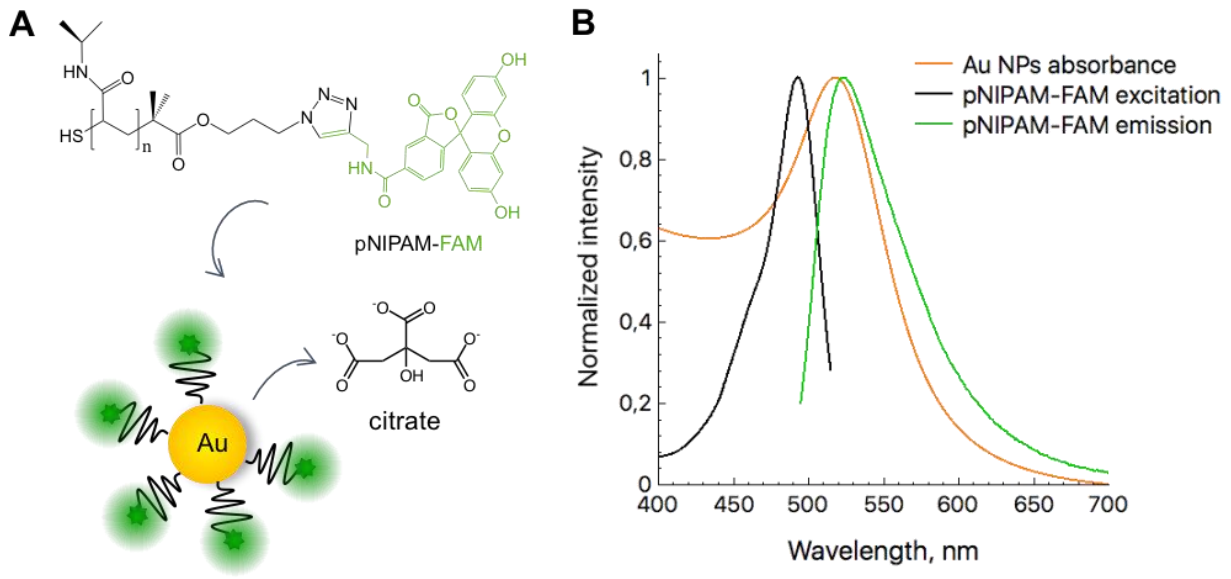

Fig. 1. pNIPAM-FAM characteristics. (A) Chemical structure of pNIPAM-FAM and schematic representation of its grafting to Au NPs stabilized with citrate. **(B)** Excitation (black) and emission (green) spectra of pNIPAM-FAM superposed with the absorbance of citrate-stabilized Au NPs (orange). **Conditions**: 20 °C, citrate-stabilized Au NPs (c_{Au0} = 0.26 mM)

diluted 5 times with water, pNIPAM-FAM solution ($c_{pNIPAM-FAM}$ = 1.8 μM) prepared in water, pNIPAM-FAM excitation at 480 nm, pNIPAM-FAM emission at 530 nm.

Au NPs were synthesized following the Turkevich method, where citrate was straightforwardly used as both reducing and stabilizing ligand (see Methods for the details of NP synthesis). [29,30] AFM imaging showed that the obtained Au NPs are uniformly spherical with average diameter of 15 ± 2 nm (Fig. S4). The resulting size of Au NPs was predetermined by the concentration of $HAuCl_4$ and the citrate : $HAuCl_4$ molar ratio, which were fixed to 0.26 mM and 6, respectively. [30] UV-visible characterization yielded maximal absorbance at 520 nm (Fig. 1B, orange), which is in the range of 519 to 522 nm previously reported for the citrate-stabilized Au NPs of similar size. [21,30,41,42] DLS measurements showed that the most probable hydrodynamic diameter of the citrate-stabilized Au NPs is 19 nm (Fig. 2A, black), which correlates with the obtained AFM (Fig. S4) and UV-visible (Fig. 1B) characteristics.

The attachment of pNIPAM-FAM to Au NPs was done through thiol/gold chemistry (see Methods for the details of the functionalization procedure). The assembly occurred through ligand exchange, in which the thiol groups of pNIPAM-FAM replaced the citrate molecules initially present at the gold surface (Fig. 1A). Fig. 2 shows characteristic DLS and UV-visible changes registered at 1 pNIPAM-FAM/nm^2 grafting density. Here, the grafting density is defined as the number of the injected molecules per nm^2 of Au surface (see Methods for the calculation of Au surface in a given volume of Au NP suspension).

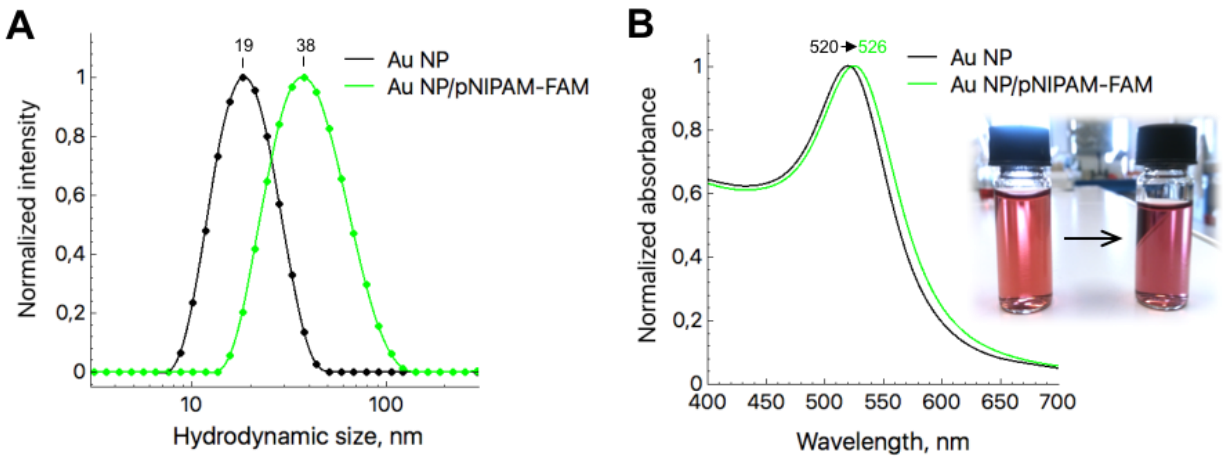

Fig. 2. Au NPs functionalization with pNIPAM-FAM. (A) Characteristic size distributions obtained by DLS before (black) and after (green) Au NPs incubation with 1 pNIPAM-FAM/nm^2. **(B)** UV-visible absorption spectra obtained for the citrate-stabilized Au NPs before (black) and after (green) their overnight incubation with 1 pNIPAM-FAM/nm^2. Inset: photo of Au NPs solution before (left) and after (right) the assembly with pNIPAM-FAM. **Conditions**: 20 °C, citrate-stabilized Au NPs (c_{Au0} = 0.26 mM) functionalized with pNIPAM-FAM ($c_{pNIPAM\text{-}FAM}$ = 1.8 μM), samples diluted 5- to 10-times with water.

We found that the average diameter of Au NPs increased from 19 ± 1 to 38 ± 2 nm after their exposure to 1 pNIPAM-FAM/nm^2, thus indicating a 10 ± 1 nm thick polymer coating (Fig. 2A). Complementary characterization by UV-visible spectroscopy showed that the absorbance maximum of the nano-assembly shifted from 520 to 526 nm (Fig. 2B). The obtained values are comparable with the reported pNIPAM thicknesses and corresponding red shifts obtained for 13 - 15 nm Au NPs functionalized with 10 kDa pNIPAM. [41,42] Taken together, UV-visible and DLS data suggest that Au NP/pNIPAM-FAM assembly is efficient at 1 pNIPAM-FAM/nm^2, even at the large excess of citrate (pNIPAM-FAM : citrate = 1 : 850).

As a further step, we studied the effect of pNIPAM-FAM grafting density on the thickness of the resulting pNIPAM-FAM coating. Fig. 3 shows the results of DLS measurements performed at different pNIPAM-FAM/nm^2 densities. We found that the average hydrodynamic size of the nano-assembly increases with the amount of injected pNIPAM-FAM. As follows from the difference before and after pNIPAM-FAM injection, varying grafting density between 0.1 and 100 pNIPAM-FAM/nm^2 allows tuning the average thickness of the pNIPAM-FAM coating in the range from 2 to 13 nm (Fig. 3). Theoretical estimation for the gyration radius of 15 kDa pNIPAM gives R_g = 5.6 nm, assuming water to be a good solvent below its transition temperature. [43] This suggests that pNIPAM-FAM adopts different conformations at the Au NP surface, varying from the mushroom-type in the diluted state (< 0.5 pNIPAM/nm^2) to the partially stretched brushes in densely-packed layers (≥ 0.5 pNIPAM/nm^2) This behavior is consisted with the mushroom-to-brush transitions reported for the acrylamide polymers end-grafted to planar metal surfaces.[44,45] The fact that the maximally achieved thickness matches the case of a slightly stretched pNIPAM brush, together with the absence of Au NPs aggregation upon pNIPAM injection (Fig. 3), suggest that non-specific interactions (e.g. pNIPAM/pNIPAM or pNIPAM/FAM) are negligible in our system.

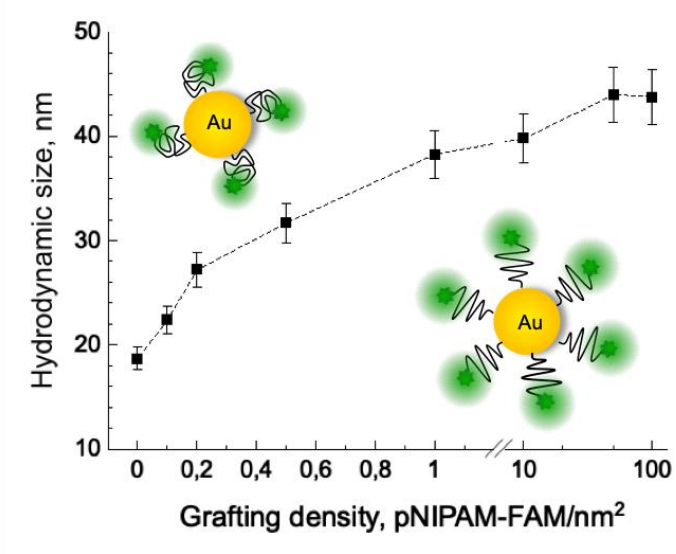

Fig. 3. Size of Au NP/pNIPAM-FAM assemblies at tunable grafting density. Average hydrodynamic sizes were determined by DLS at different pNIPAM-FAM/nm^2 ratios by interpolating the registered size distributions as exampled by Fig. 2A. Standard errors were determined by averaging data of 3 samples having the same grafting density (Table S1). Schematics of Au NP/pNIPAM-FAM assemblies at low (< 0.5 pNIPAM/nm^2) and high (≥ 0.5 pNIPAM/nm^2) grafting densities are shown on the left and on the right, respectively. **Conditions**: 20 °C, citrate-stabilized Au NPs (c_{Au0} = 0.26 mM) functionalized with pNIPAM-FAM ($c_{pNIPAM\text{-}FAM}$ = 0.18 – 176.13 μM), samples diluted 5- to 10-times with water.

Given that the most drastic increase in the pNIPAM-FAM thickness occurs between 0.1 and 1 pNIPAM-FAM/nm^2 (from 0 to 80 % of its maximal value, Fig. 3), we performed subsequent fluorescence characterization in this range. Generally, 100-times higher pNIPAM/nm^2 ratios are used for Au NPs functionalization, followed by Au NPs purification from the excess of free pNIPAM, [21,41,46] with the need to use harsh conditions such as organic solvents being emphasized. [46] To avoid potential impact of those on colloidal stability and/or optical characteristics, we decreased the initial amount of pNIPAM-FAM to 0.1 - 1 ligands/nm^2 and

characterized the obtained Au NP/pNIPAM-FAM assemblies as prepared, assuming the majority of pNIPAM-FAM to be end-grafted to Au NPs. Complementary SPR experiments on planar gold substrates were performed to estimate the number of the attached pNIPAM-FAM per surface area. The obtained value of 0.4 pNIPAM-FAM/nm^2 is within the range of 0.1 - 1 ligands/nm^2, supporting our assumption (see Supplementary Information for the details of SPR measurements).

The superposition of optical characteristics of pNIPAM-FAM and Au NPs shows a strong overlap between pNIPAM-FAM emission and Au NPs plasmon band (Fig. 1B). Taking into account the high quantum yield of FAM emission and relatively small size of Au NPs, one should expect fluorescence quenching upon Au NP/pNIPAM-FAM coupling, and the thinner is the pNIPAM coating the stronger should be the resulting quenching. [4] To verify this, we characterized pNIPAM-FAM fluorescence before and after its assembly with Au NPs, while tuning pNIPAM-FAM grafting density between 0.1 and 1 pNIPAM-FAM/nm^2. Characteristic excitation and emission spectra obtained at 1 pNIPAM-FAM/nm^2 are shown in Fig. 4A. The resulting quenching and its dependence on grafting density are shown in Fig. 4B.

These results suggest that fluorescence quenching is indeed strong in our system, reaching 80 % in diluted pNIPAM coatings ($\leq$ 0.2 pNIPAM-FAM/nm^2), i.e. where pNIPAM chains are the least stretched. As expected, quenching decreased with the thickness of the pNIPAM-FAM layer: 60 % efficiency was registered at 1 pNIPAM-FAM/nm^2 ratio, corresponding to the partially stretched pNIPAM brush. At > 1 pNIPAM/nm^2, the potential impact of Au NPs on the fluorescence of free pNIPAM-FAM should be negligible due to the sufficient thickness of the pNIPAM coating (Fig. 3). The fact that quenching remains strong at 1 pNIPAM-FAM/nm^2, while being much weaker at higher grafting densities (24 and 9 % were obtained for 10 and 50

pNIPAM-FAM/nm^2, Fig. S5), supports our assumption that most of pNIPAM-FAM is attached to Au NPs at grafting densities ≤ 1 pNIPAM/nm^2. In addition, fluorescence analysis of dialyzed samples showed that < 20 % of pNIPAM-FAM is unbound at 1 pNIPAM-FAM/nm^2, which further validates this assumption (see Supplementary Information and Fig. S6 for the details of dialysis experiment).

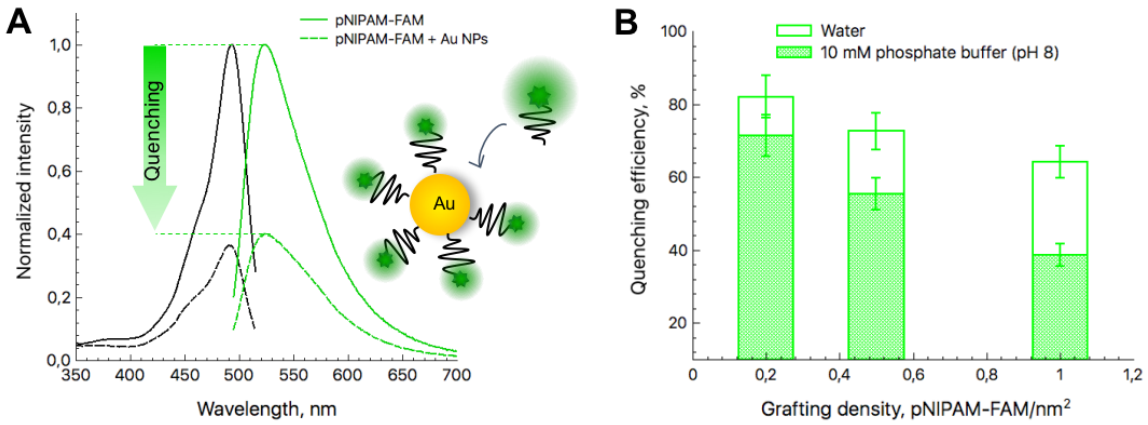

Fig. 4. Fluorescence properties of Au NP/pNIPAM-FAM assemblies. (A) Excitation (black) and emission (green) spectra of pNIPAM-FAM obtained in the absence (solid lines) and in the presence (dashed lines) of Au NPs. Data correspond to 1 pNIPAM-FAM/nm^2 ratio; the resulting quenching is depicted by the rightmost empty green column in (B). **(B)** Fluorescence characteristics obtained for 0.1, 0.5 and 1 pNIPAM-FAM/nm^2 grafting densities. Quenching efficiency was calculated as $Q = (I_{max} - I_{max}^{Au\,NP}) \times 100\,\%/I_{max}$, where I_{max} and $I_{max}^{Au\,NP}$ are the maximal intensities of pNIPAM-FAM emission in the absence and in the presence of Au NPs. Standard errors were determined by averaging data of 3 samples having the same grafting density. **Conditions**: 20 °C, citrate-stabilized Au NPs (c_{Au0} = 0.26 mM) functionalized with pNIPAM-FAM ($c_{pNIPAM\text{-}FAM}$ = 0.36 – 1.76 μM), samples diluted 5-to 10-times with water (empty

columns) or 10 mM sodium phosphate buffer, pH = 8 (filled columns), pNIPAM-FAM excitation at 480 nm, pNIPAM-FAM emission at 530 nm.

The common quenching mechanisms, such as Förster Resonance Energy Transfer (FRET) and Surface Energy Transfer (SET), suggest that at distances below ~ 10 nm, fluorescence increases supra-linearly with d (FRET $\propto 1/d^6$, SET $\propto 1/d^4$). [47] It was already observed in static systems that the experimentally derived dependence of fluorescence quenching on Au NP/FAM separation is less pronounced than the theoretical prediction. [5] One reason for this could be the tendency of the end-grafted FAM to intercalate into the underlying polymer layer. In order to promote FAM exposure into the solution, we increased its hydrophilicity by transferring Au NP/pNIPAM-FAM assemblies into 10 mM sodium phosphate buffer at pH 8. Buffer concentration and pH were chosen to minimize their effect on the Au NP/pNIPAM colloidal properties.[48,49] Control experiments at 0 and 0.5 pNIPAM-FAM/nm^2 grafting densities confirmed that the size and the stability of the synthesized nano-assemblies are not affected by the induced pH and ionic strength changes (Fig. S7, Table S1). The measured in 10 mM phosphate buffer (pH 8) quenching of FAM emission decreased to 39 % as compared to 60% registered for dense pNIPAM brushes in water, with similar tendency being observed for other grafting densities (Fig. 4B), suggesting indeed better Au NP/FAM separation under these conditions.

Thermo-responsive properties of Au NP/pNIPAM-FAM assemblies were characterized while varying grafting density between 0.1 and 1 pNIPAM-FAM/nm^2. DLS and fluorescence characterizations were performed at 20 and 40 °C, i.e. below and above the expected pNIPAM transition temperature. [50] DLS and fluorescence measurements were performed on the same samples in parallel, which allowed to correlate variations in the size of the assemblies with the changes in their fluorescence intensity. The obtained results are summarized in Fig. 5. In contrast

to the majority of nano-assemblies obtained by grafting thermo-responsive polymers to Au NPs, we did not observe Au NP/pNIPAM-FAM aggregation upon heating. [51] Given the promoting role of free pNIPAM chains in the aggregation of pNIPAM-coated particles, [46] the observed stability may be due to the low amount of unbound pNIPAM-FAM in 0.1 - 1 pNIPAM-FAM/nm^2 samples, together with the excess of citrate (850 ligands/nm^2), which may additionally stabilize assemblies above LCST. [51,52] In order to verify the role of free pNIPAM in the Au NP/pNIPAM aggregation, we compared DLS results obtained for pNIPAM-FAM and Au NP/pNIPAM-FAM samples at 1 and 10 pNIPAM-FAM/nm^2. In the case of 1 pNIPAM-FAM/nm^2, no aggregation was detected for the Au NP/pNIPAM-FAM sample, whereas ~ 150 nm aggregates were observed upon heating of free pNIPAM-FAM at the same concentration (Fig. S8A). When the grafting density was increased to 10 pNIPAM-FAM/nm^2, both pNIPAM-FAM and Au NP/pNIPAM-FAM samples showed aggregation (Fig. S8A, B, Table S1). These results agree with fluorescence data (Figs. 4, S5, S6), confirming the low amount of unbound pNIPAM-FAM at grafting densities $\leq$ 1 ligands/nm^2.

Characteristic size distributions obtained at 1 pNIPAM-FAM/nm^2 indicate reversible shrinking of Au NP/pNIPAM-FAM assemblies upon heating, with similar behavior being observed at other grafting densities (Figs. 5A, B, S9B). The repeatability of temperature-driven size modulations is illustrated in Fig. S9A. The growth of size variation with grafting density can be explained by stronger contribution of pNIPAM-FAM (*versus* initial citrate coating) into the average hydrodynamic size as well as by sharper pNIPAM-FAM transition from a partially stretched brush to a collapsed coil conformation. [43,51] The observed small variation at 0.2 pNIPAM/nm^2 indicates that in the mushroom regime, pNIPAM chains have somewhat different

conformation below and above LCST, with transition being presumably driven by partially present steric effects. [51]

Fluorescence change kinetics recorded in parallel shows that Au NP/pNIPAM-FAM emission decreases after heating and increases after cooling back to room temperature (Fig. 5C). Given that fluorescence fluctuations did not exceed 6 % in the case of free pNIPAM-FAM (Fig. S9C inset), the registered fluorescence modulations of 12 to 18 % can be attributed to the temperature-driven shrinking of Au NP/pNIPAM-FAM assemblies. The cyclability of the fluorescence modulation is illustrated in Fig. S9A, C. The slight increase in fluorescence emission after each cycle (Fig. 5C, Fig. S9C) could be attributed to the re-arrangements in the pNIPAM-FAM brush[51] and/or release of a small fraction of pNIPAM-FAM from the surface of Au NPs. [53] The proposed mechanism of fluorescence switching is schematically shown in Fig. 5A (inset). The average Au NP/FAM distance decreases upon pNIPAM shrinking, resulting in stronger fluorescence quenching, and *vice versa*, which allows reversible fluorescence switching in response to external heating.

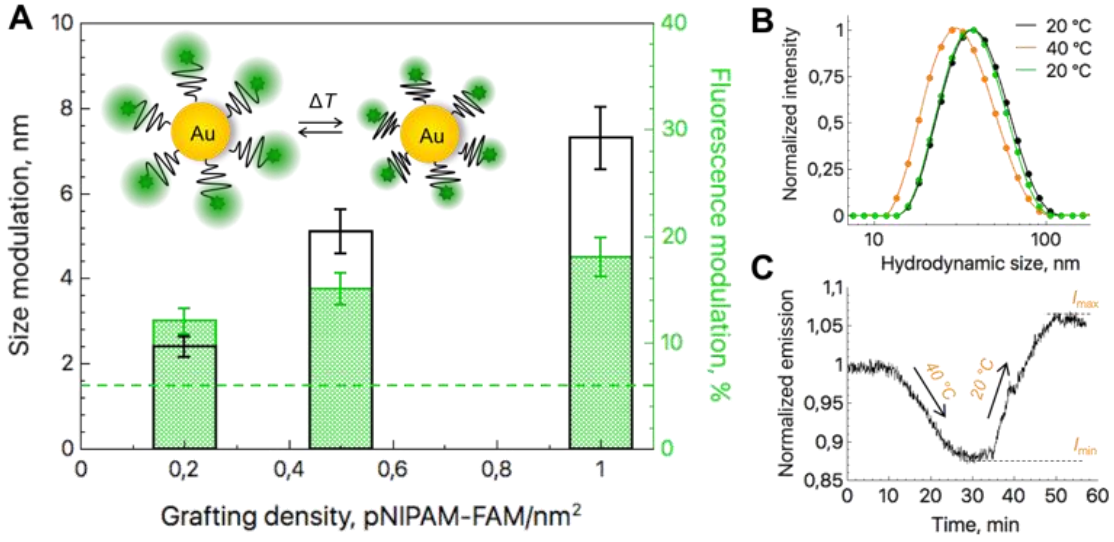

Fig. 5. Thermoresponsive behavior of Au NP/pNIPAM-FAM assemblies. (A) Changes in hydrodynamic size (left, black columns) and fluorescence emission (right, green columns) in response to temperature switching between 20 and 40 °C, registered at different pNIPAM-FAM/nm^2 ratios. Dashed green line indicates fluorescence variations recorded for pNIPAM-FAM in the absence of Au NPs. Size modulations are calculated as $\Delta D_h = D_h^{20\,^\circ C} - D_h^{40\,^\circ C}$, where $D_h^{20\,^\circ C}$and $D_h^{40\,^\circ C}$ are the average hydrodynamic sizes at 20 and 40 °C determined from size distributions ($D_h^{20\,^\circ C}$and $D_h^{40\,^\circ C}$ values are provided in Table S1); relative fluorescence changes are calculated as $\Delta I = (I_{max} - I_{min}) \times 100\,\%/I_{max}$, where I_{max} and I_{min} are the maximal and minimal fluorescence intensities recorded during kinetics measurements. Inset: schematic representation of temperature-driven shrinking of Au NP/pNIPAM-FAM assemblies inducing reversible fluorescence modulation. **(B)** Characteristic size distributions registered at 1 pNIPAM-FAM/nm^2 grafting density upon changing temperature from 20 (black) to 40 °C (orange) and back to 20 °C (green). **(C)** Characteristic fluorescence kinetics at 1 pNIPAM-FAM/nm^2 in response to sequential 20/40/20 °C temperature switching. **Conditions**: temperature varied between 20 and 40 °C, citrate-stabilized Au NPs (c_{Au0} = 0.26 mM) functionalized with pNIPAM-FAM ($c_{\mathrm{pNIPAM\text{-}FAM}}$ = 0.36 – 1.76 μM), samples diluted 5-to 10-times with water (DLS measurements) or with 10 mM sodium phosphate buffer, pH = 8 (fluorescence kinetics), pNIPAM-FAM excitation at 465 nm, pNIPAM-FAM emission at 530 nm.

CONCLUSIONS

We have presented a dynamic plasmonic system allowing reversible fluorescence switching *via* external control of the Au NP/fluorophore distance. As a proof of concept, Au NPs were functionalized with thermo-responsive pNIPAM displaying FAM at the solution-facing end. We

showed that the resulting thickness of the pNIPAM coating can be precisely tuned by choosing appropriate pNIPAM grafting density. Furthermore, we demonstrated that fluorescence emission of the obtained Au NP/pNIPAM-FAM assemblies can be switched on-demand in response to external heating, which was attributed to the reversible shrinking of pNIPAM. Our work is in progress to extend this concept to thermo-responsive polymers having adjustable transition temperature and to study the possibility of combining plasmonic heating with local temperature sensing. The developed strategy is compatible with various plasmonic nanostructures and fluorophores and can be adapted for other external stimuli. It therefore holds significant potential for nanotechnology, in particular for biological and chemical sensing applications where multi-functional fluorescence detection is demanded at the nano-scale.

ASSOCIATED CONTENT

Supporting Information. Characterization of pNIPAM-FAM by UV-visible and fluorescence spectroscopy, characterization of Au NPs by AFM, characterization of Au NP/pNIPAM-FAM assemblies by DLS and fluorescence spectroscopy, SPR characterization of pNIPAM-FAM surface density.

AUTHOR INFORMATION

Corresponding Author

Galina Dubacheva − Department of Molecular Chemistry, Université Grenoble Alpes, CNRS UMR 5250, Grenoble 38000, France; orcid.org/0000-0003-1417-5381; Email: galina.dubacheva@univ-grenoble-alpes.fr.

Notes

The authors declare no competing financial interest.

ACKNOWLEDGMENT

This work was supported by ANR JCJC "SupraSwitch" (ANR-18-CE09-0009) and LabEx "Charmmmat" (ANR-11-LABX-0039). H. Bonnet (DCM, UGA) is acknowledged for help with SPR measurements.

REFERENCES

(1) Sardar, R.; Funston, A. M.; Mulvaney, P.; Murray, R. W. Gold Nanoparticles: Past, Present, and Future. *Langmuir* **2009**, *25* (24), 13840–13851.

(2) Saha, K.; Agasti, S. S.; Kim, C.; Li, X.; Rotello, V. M. Gold Nanoparticles in Chemical and Biological Sensing. *Chem. Rev.* **2012**, *112* (5), 2739–2779.

(3) Howes, P. D.; Rana, S.; Stevens, M. M. Plasmonic Nanomaterials for Biodiagnostics. *Chem. Soc. Rev.* **2014**, *43* (11), 3835–3853.

(4) *Principles of Fluorescence Spectroscopy*; Lakowicz, J. R., Ed.; Springer US: Boston, MA, 2006.

(5) Kang, K. A.; Wang, J.; Jasinski, J. B.; Achilefu, S. Fluorescence Manipulation by Gold Nanoparticles: From Complete Quenching to Extensive Enhancement. *J. Nanobiotechnology* **2011**, *9*, 16.

(6) Yuan, H.; Khatua, S.; Zijlstra, P.; Yorulmaz, M.; Orrit, M. Thousand-Fold Enhancement of Single-Molecule Fluorescence Near a Single Gold Nanorod. *Angew. Chem. Int. Ed.* **2013**, *52* (4), 1217–1221.

(7) Klajn, R.; Stoddart, J. F.; Grzybowski, B. A. Nanoparticles Functionalised with Reversible Molecular and Supramolecular Switches. *Chem. Soc. Rev.* **2010**, *39* (6), 2203–2237.

(8) Becker, K.; Lupton, J. M.; Müller, J.; Rogach, A. L.; Talapin, D. V.; Weller, H.; Feldmann, J. Electrical Control of Förster Energy Transfer. *Nat. Mater.* **2006**, *5* (10), 777–781.

(9) Guerret, L.; Audibert, J.-F.; Debarre, A.; Lepeltier, M.; Haghi-Ashtiani, P.; Dubacheva, G. V.; Miomandre, F. Investigation of Photophysical and Electrofluorochromic Properties of Gold Nanoparticles Functionalized by a Luminescent Electroactive Complex. *J. Phys. Chem. C* **2016**, *120* (4), 2411–2418.

(10) Zhu, L.; Zhu, M.-Q.; Hurst, J. K.; Li, A. D. Q. Light-Controlled Molecular Switches Modulate Nanocrystal Fluorescence. *J. Am. Chem. Soc.* **2005**, *127* (25), 8968–8970.

(11) Miranda, O. R.; Creran, B.; Rotello, V. M. Array-Based Sensing with Nanoparticles: "Chemical Noses" for Sensing Biomolecules and Cell Surfaces. *Curr. Opin. Chem. Biol.* **2010**, *14* (6), 728–736.

(12) Ohta, S.; Glancy, D.; Chan, W. C. W. DNA-Controlled Dynamic Colloidal Nanoparticle Systems for Mediating Cellular Interaction. *Science* **2016**, *351* (6275), 841–845.

(13) Álvarez-Puebla, R. A.; Contreras-Cáceres, R.; Pastoriza-Santos, I.; Pérez-Juste, J.; Liz-Marzán, L. M. Au@pNIPAM Colloids as Molecular Traps for Surface-Enhanced, Spectroscopic, Ultra-Sensitive Analysis. *Angew. Chem. Int. Ed.* **2009**, *48* (1), 138–143.

(14) Turek, V. A.; Chikkaraddy, R.; Cormier, S.; Stockham, B.; Ding, T.; Keyser, U. F.; Baumberg, J. J. Thermo-Responsive Actuation of a DNA Origami Flexor. *Adv. Funct. Mater.* **2018**, *28* (25), 1706410.

(15) Wongkongkatep, J.; Ladadat, R.; Lappermpunsap, W.; Wongkongkatep, P.; Phinyocheep, P.; Ojida, A.; Hamachi, I. Thermoresponsive Fluorescent Sensor Based on Core/Shell Nanocomposite Composed of Gold Nanoparticles and Poly(N-Isopropylacrylamide). *Chem. Lett.* **2010**, *39* (3), 184–185.

(16) Sugawa, K.; Ichikawa, R.; Takeshima, N.; Tanoue, Y.; Otsuki, J. Development of Highly Thermoresponsive Fluorescent Sensors Consisting of Plasmonic Silver Nanoprisms and Poly(N-Isopropylacrylamide)–Fluorophore Composites. *Photochem. Photobiol. Sci.* **2015**, *14* (5), 870–874.

(17) Gandhi, A.; Paul, A.; Sen, S. O.; Sen, K. K. Studies on Thermoresponsive Polymers: Phase Behaviour, Drug Delivery and Biomedical Applications. *Asian J. Pharm. Sci.* **2015**, *10* (2), 99–107.

(18) Guan, Y.; Zhang, Y. PNIPAM Microgels for Biomedical Applications: From Dispersed Particles to 3D Assemblies. *Soft Matter* **2011**, *7* (14), 6375–6384.

(19) Dalier, F.; Dubacheva, G. V.; Coniel, M.; Zanchi, D.; Galtayries, A.; Piel, M.; Marie, E.; Tribet, C. Mixed Copolymer Adlayers Allowing Reversible Thermal Control of Single Cell Aspect Ratio. *ACS Appl Mater Interfaces* **2018**, *10* (3), 2253–2258.

(20) Kearns, H.; Shand, N. C.; Faulds, K.; Graham, D. Laser Induced SERS Switching Using Plasmonic Heating of PNIPAM Coated HGNs. *Chem. Commun.* **2015**, *51* (38), 8138–8141.

(21) Kusolkamabot, K.; Sae-ung, P.; Niamnont, N.; Wongravee, K.; Sukwattanasinitt, M.; Hoven, V. P. Poly(N-Isopropylacrylamide)-Stabilized Gold Nanoparticles in Combination with Tricationic Branched Phenylene-Ethynylene Fluorophore for Protein Identification. *Langmuir* **2013**, *29* (39), 12317–12327.

(22) Kim, J.; Serpe, M. J.; Lyon, L. A. Photoswitchable Microlens Arrays. *Angew. Chem. Int. Ed.* **2005**, *44* (9), 1333–1336.

(23) Suzuki, D.; McGrath, J. G.; Kawaguchi, H.; Lyon, L. A. Colloidal Crystals of Thermosensitive, Core/Shell Hybrid Microgels. *J. Phys. Chem. C* **2007**, *111* (15), 5667–5672.

(24) Ding, T.; J. Baumberg, J. Thermo-Responsive Plasmonic Systems: Old Materials with New Applications. *Nanoscale Adv.* **2020**, *2* (4), 1410–1416.

(25) Deng, F.; Wang, Y.; Lu, X.; Ding, T. Probing Hidden Colloidal Transitions with the Assistance of Surface Plasmons. *Phys. Chem. Chem. Phys.* **2019**, *21* (28), 15742–15746.

(26) Zhang, C.; Deng, F.; Xiong, W.; Wang, X.; Yuan, S.; Ding, T. Thermally-Driven Gold@poly(N-Isopropylacrylamide) Core-Shell Nanotransporters for Molecular Extraction. *J. Colloid Interface Sci.* **2021**, *584*, 789–794.

(27) Tang, F.; Ma, N.; Wang, X.; He, F.; Li, L. Hybrid Conjugated Polymer-Ag@PNIPAM Fluorescent Nanoparticles with Metal-Enhanced Fluorescence. *J. Mater. Chem.* **2011**, *21* (42), 16943–16948.

(28) Yan, F.; Fan, K.; Bai, Z.; Zhang, R.; Zu, F.; Xu, J.; Li, X. Fluorescein Applications as Fluorescent Probes for the Detection of Analytes. *TrAC Trends Anal. Chem.* **2017**, *97*, 15–35.

(29) Ziegler, C.; Eychmuller, A. Seeded Growth Synthesis of Uniform Gold Nanoparticles with Diameters of 15-300 Nm. *J Phys Chem C* **2011**, *115*, 4502–4506.

(30) Ojea-Jiménez, I.; Bastús, N. G.; Puntes, V. Influence of the Sequence of the Reagents Addition in the Citrate-Mediated Synthesis of Gold Nanoparticles. *J. Phys. Chem. C* **2011**, *115* (32), 15752–15757.

(31) Scarabelli, L.; Sánchez-Iglesias, A.; Pérez-Juste, J.; Liz-Marzán, L. M. A "Tips and

Tricks" Practical Guide to the Synthesis of Gold Nanorods. *J. Phys. Chem. Lett.* **2015**, *6* (21), 4270–4279.

(32) Liu, X.; Atwater, M.; Wang, J.; Huo, Q. Extinction Coefficient of Gold Nanoparticles with Different Sizes and Different Capping Ligands. *Colloids Surf. B Biointerfaces* **2007**, *58* (1), 3–7.

(33) Said Hassane, F.; Frisch, B.; Schuber, F. Targeted Liposomes: Convenient Coupling of Ligands to Preformed Vesicles Using "Click Chemistry." *Bioconjug. Chem.* **2006**, *17* (3), 849–854.

(34) Meldal, M.; Tornøe, C. W. Cu-Catalyzed Azide−Alkyne Cycloaddition. *Chem. Rev.* **2008**, *108* (8), 2952–3015.

(35) Hein, J. E.; Fokin, V. V. Copper-Catalyzed Azide–Alkyne Cycloaddition (CuAAC) and beyond: New Reactivity of Copper(I) Acetylides. *Chem. Soc. Rev.* **2010**, *39* (4), 1302–1315.

(36) Dalier, F.; Dubacheva, G. V.; Coniel, M.; Zanchi, D.; Galtayries, A.; Piel, M.; Marie, E.; Tribet, C. Mixed Copolymer Adlayers Allowing Reversible Thermal Control of Single Cell Aspect Ratio. *ACS Appl. Mater. Interfaces* **2018**, *10* (3), 2253–2258.

(37) Dalier, F.; Eghiaian, F.; Scheuring, S.; Marie, E.; Tribet, C. Temperature-Switchable Control of Ligand Display on Adlayers of Mixed Poly(Lysine)-g-(PEO) and Poly(Lysine)-g-(Ligand-Modified Poly-N-Isopropylacrylamide). *Biomacromolecules* **2016**, *17* (5), 1727–1736.

(38) Sjöback, R.; Nygren, J.; Kubista, M. Characterization of Fluorescein-Oligonucleotide Conjugates and Measurement of Local Electrostatic Potential. *Biopolymers* **1998**, *46* (7), 445–453.

(39) Kim, M.; Schmitt, S. K.; Choi, J. W.; Krutty, J. D.; Gopalan, P. From Self-Assembled Monolayers to Coatings: Advances in the Synthesis and Nanobio Applications of Polymer Brushes. *Polymers* **2015**, *7* (7), 1346–1378.

(40) Said Hassane, F.; Frisch, B.; Schuber, F. Targeted Liposomes: Convenient Coupling of Ligands to Preformed Vesicles Using "Click Chemistry." *Bioconjug. Chem.* **2006**, *17* (3), 849–854.

(41) Liu, F.; Cui, Y.; Wang, L.; Wang, H.; Yuan, Y.; Pan, J.; Chen, H.; Yuan, L. Temperature-Responsive Poly(N-Isopropylacrylamide) Modified Gold Nanoparticle-Protein Conjugates for Bioactivity Modulation. *ACS Appl. Mater. Interfaces* **2015**, *7* (21), 11547–11554.

(42) Maji, S.; Cesur, B.; Zhang, Z.; Geest, B. G. D.; Hoogenboom, R. Poly(N -Isopropylacrylamide) Coated Gold Nanoparticles as Colourimetric Temperature and Salt Sensors. *Polym. Chem.* **2016**, *7* (9), 1705–1710.

(43) Jalili, K.; Abbasi, F.; Milchev, A. Surface Microdynamics Phase Transition and Internal Structure of High-Density, Ultrathin PHEMA-b-PNIPAM Diblock Copolymer Brushes on Silicone Rubber. *Macromolecules* **2013**, *46* (13), 5260–5278.

(44) Liu, G.; Cheng, H.; Yan, L.; Zhang, G. Study of the Kinetics of the Pancake-to-Brush

Transition of Poly(N-Isopropylacrylamide) Chains. *J. Phys. Chem. B* **2005**, *109* (47), 22603–22607.

(45) Wu, T.; Efimenko, K.; Genzer, J. Combinatorial Study of the Mushroom-to-Brush Crossover in Surface Anchored Polyacrylamide. *J. Am. Chem. Soc.* **2002**, *124* (32), 9394–9395.

(46) Jones, S. T.; Walsh-Korb, Z.; Barrow, S. J.; Henderson, S. L.; del Barrio, J.; Scherman, O. A. The Importance of Excess Poly(N-Isopropylacrylamide) for the Aggregation of Poly(N-Isopropylacrylamide)-Coated Gold Nanoparticles. *ACS Nano* **2016**, *10* (3), 3158–3165.

(47) Sen, T.; Patra, A. Recent Advances in Energy Transfer Processes in Gold-Nanoparticle-Based Assemblies. *J. Phys. Chem. C* **2012**, *116* (33), 17307–17317.

(48) Willott, J. D.; Humphreys, B. A.; Murdoch, T. J.; Edmondson, S.; Webber, G. B.; Wanless, E. J. Hydrophobic Effects within the Dynamic PH-Response of Polybasic Tertiary Amine Methacrylate Brushes. *Phys. Chem. Chem. Phys.* **2015**, *17* (5), 3880–3890.

(49) Humphreys, B. A.; Wanless, E. J.; Webber, G. B. Effect of Ionic Strength and Salt Identity on Poly(N-Isopropylacrylamide) Brush Modified Colloidal Silica Particles. *J. Colloid Interface Sci.* **2018**, *516*, 153–161.

(50) Ren, H.; Qiu, X.-P.; Shi, Y.; Yang, P.; Winnik, F. M. The Two Phase Transitions of Hydrophobically End-Capped Poly(N-Isopropylacrylamide)s in Water. *Macromolecules* **2020**, *53* (13), 5105–5115.

(51) Gibson, M. I.; O'Reilly, R. K. To Aggregate, or Not to Aggregate? Considerations in the Design and Application of Polymeric Thermally-Responsive Nanoparticles. *Chem. Soc. Rev.* **2013**, *42* (17), 7204–7213.

(52) Mastrotto, F.; Caliceti, P.; Amendola, V.; Bersani, S.; Magnusson, J. P.; Meneghetti, M.; Mantovani, G.; Alexander, C.; Salmaso, S. Polymer Control of Ligand Display on Gold Nanoparticles for Multimodal Switchable Cell Targeting. *Chem. Commun.* **2011**, *47* (35), 9846–9848.

(53) Borzenkov, M.; Chirico, G.; D'Alfonso, L.; Sironi, L.; Collini, M.; Cabrini, E.; Dacarro, G.; Milanese, C.; Pallavicini, P.; Taglietti, A.; Bernhard, C.; Denat, F. Thermal and Chemical Stability of Thiol Bonding on Gold Nanostars. *Langmuir* **2015**, *31* (29), 8081–8091.

Table of Contents Graphic